CrossMark

Induction of apoptosis in SGC-7901 cells by ruthenium(II) complexes through ROS-mediated lysosome–mitochondria dysfunction and inhibition of PI3K/AKT/mTOR pathways

Qiao-Yan Yi[1] · Yang-Jie Wang[1] · Miao He[1] · Wen-Yao Zhang[1] · Fan Du[1] · Yi-Ying Gu[1] · Lan Bai[1] · Yun-Jun Liu[1]

Abstract

Five Ru(II) polypyridyl complexes $[Ru(N–N)_2(nfip)](ClO_4)_2$ (N–N = dmb, **1**; bpy, **2**; ttbpy, **3**, phen, **4**, dmp, **5**) were synthesized and characterized. The cytotoxic activities of the complexes against cancer SGC-7901, Eca-109, HepG2, A549, HeLa and normal LO2 cells were investigated using the MTT method. Complexes **1**–**4** show high cytotoxicity against SGC-7901 cells with low IC_{50} values of 12.4 ± 1.4, 6.7 ± 1.6, 1.3 ± 0.5 and 1.1 ± 0.4 μM, respectively. Complex **5** is active against HeLa cells with an IC_{50} value of 2.2 ± 0.6 μM. Among these complexes, complexes **3** and **4** exhibit higher cytotoxic activity than cisplatin toward SGC-7901 cells under identical conditions. Apoptosis was assayed using the AO/EB staining method and flow cytometry. The location of the complexes at lysosomes and mitochondria, the permeability of lysosomes, the levels of reactive oxygen species, and the changes of mitochondrial membrane potential were studied by fluorescence microscopy. The cell cycle distribution of SGC-7901 cells induced by the complexes was studied by flow cytometry. The expression of caspase-3, PARP and Bcl-2 family proteins was investigated by Western blot. The complexes were shown to accumulate in the lysosomes and then enter into the mitochondria. The mechanism demonstrates that the complexes induce apoptosis in SGC-7901 cells through three pathways: (1) ROS-mediated lysosomal–mitochondrial dysfunction; (2) inhibition of PI3K/AKT/mTOR pathway; and (3) DNA damage and inhibition of the cell growth at G0/G1 or S phase.

Introduction

Transition metal compounds have been widely used as chemotherapeutic agents in the treatment of several types of malignancies, such as colon, lung and breast cancers. By virtue of their ability to modulate various biological processes involving DNA, metal complexes have received considerable attention as potential anticancer agents [1, 2]. The discovery of the anticancer properties of cisplatin brought a significant improvement in cancer treatment. Several other cisplatin analogues, including carboplatin, oxaliplatin, nedaplatin, heptaplatin and lobaplatin, were developed as a result of further experimentation. These drugs cause many side

effects like nephrotoxicity, neurotoxicity, gastrointestinal toxicity [3, 4]. In an attempt to solve these problems, there has been continuous interest in alternative metal-based complexes. Among them Ru(II) polypyridyl complexes offer facile synthesis and possess agreeable chemical, physical and photophysical characteristics. In recent years, the anticancer activity of Ru(II) polypyridyl complexes has been paid great attention and some interesting properties have been obtained [5–20]. The complex $[Ru(dmp)_2(PTTP)](ClO_4)_2$ can effectively inhibit the growth of BEL-7402 cells with a low IC_{50} value of 2.2 ± 0.2 μM [21]. $[Ru(dmp)_2(pddppn)](ClO_4)_2$ displays high inhibitory efficiency against BEL-7402, MG-63 and A549 cells; the complex induces cell cycle arrest at G2/M phase against BEL-7402 and MG-63 cells, at G0/G1 phase at S phase, and causes apoptosis through ROS-mediated mitochondrial dysfunction pathway [22]. Chen et al. reported that RuPOP, a ruthenium polypyridyl complex with potent antitumor activity, was able to effectively inhibit growth and metastasis of MDA-MB-231 cells and synergistically enhance TRAIL-induced apoptosis [23]. The complexes $[Ru(phen)_2(bppp)]^{2+}$ and $[Ru(phen)_2(7\text{-Br-}dppz)]^{2+}$ show prominent anticancer activity against various

✉ Yun-Jun Liu
  lyjche@gdpu.edu.cn

1 School of Pharmacy, Guangdong Pharmaceutical University, Guangzhou 510006, People's Republic of China

cancer cells. Live cell imaging study demonstrates that the two complexes could cross the cell membrane, accumulating in the nuclei [24]. Owing to Ru(II) polypyridyl complexes having a diversity of chemical structures that are readily available through modification of coordinating ligands [25], this structural diversity of the complexes makes them significantly useful as biological probes and effectors [26]. Chao et al. reported that the complexes Δ-[Ru(bpy)$_2$(nfip)]$^{2+}$ and Λ-[Ru(bpy)$_2$(nfip)]$^{2+}$ show large DNA-binding affinities, and the DNA-binding constants are 7.0×10^5 and 6.3×10^5, respectively [27]. This prompted us to explore cancer activity of complexes with nfip ligands. In order to obtain an accurate and deep understanding the anticancer activity of Ru(II) polypyridyl complexes, in this article, five Ru(II) polypyridyl complexes [Ru(dmb)$_2$(nfip)](ClO$_4$)$_2$ **1** (dmb = 4,4′-dimethyl-2,2′-bipyridine), [Ru(bpy)$_2$(nfip)] (ClO$_4$)$_2$ **2** (bpy = 2,2′-bipyridine), [Ru(ttbpy)$_2$(nfip)] (ClO$_4$)$_2$ **3** (ttbpy = 4,4′-ditertiary butyl-2,2′-bipyridine), [Ru(phen)$_2$(nfip)](ClO$_4$)$_2$ **4** (phen = 1,10-phenanthroline) and [Ru(dmp)$_2$(nfip)](ClO$_4$)$_2$ **5** (dmp = 2,9-dimethyl-1,10-phenanthroline, nfip = 2-(5-nitrofuran-2-yl)-1*H*-imidazo[4,5-f] [1,10]phenanthroline) shown in Scheme 1 were synthesized and characterized by elemental analysis, IR, ESI–MS, ^{1}H NMR and ^{13}C NMR. The in vitro cytotoxic activity of the complexes against SGC-7901, Eca-109, HepG2, A549, HeLa and normal LO2 cells was investigated using the MTT (3-(4,5-dimethylthiazole)-2,5-diphenyltetrazolium bromide) method. The results demonstrated that the complexes induced SGC-7901 cell apoptosis by acting on lysosomal–mitochondrial dysfunction and inhibition of PI3K/AKT/mTOR pathways.

Experimental

Materials and methods

All reagents and solvents were purchased commercially and used without further purification unless otherwise noted. Ultrapure Milli-Q water was used in all experiments. RPMI 1640 was purchased from Sigma. 1,10-Phenanthroline was obtained from the Guangzhou Chemical Reagent Factory. The cancer cell lines of SGC-7901 (human gastric adenocarcinoma), HeLa (human cervical cancer), Eca-109 (human esophageal cancer cell), A549 (human lung carcinoma) and HepG2 (human hepatocellular carcinoma), and normal LO2 cells (human liver cells) were purchased from the American Type Culture Collection. RuCl$_3$·3H$_2$O was purchased from the Kunming Institution of Precious Metals. Microanalysis (C, H, and N) was carried out with a PerkinElmer 240Q elemental analyzer. Electrospray ionization mass spectra (ESI–MS) were recorded on a LCQ system (Finnigan MAT, USA) using acetonitrile as the mobile phase. The spray voltage, tube lens offset, capillary voltage and capillary temperature were set at 4.50 kV, 30.00 V, 23.00 V and 200 °C, respectively, and the quoted m/z values are for the major peaks in the isotope distribution. ^{1}H NMR and ^{13}C NMR spectra were recorded on a Varian-500 spectrometer with DMSO-d6 as a solvent and tetramethylsilane (TMS) as an internal standard at 500 MHz at room temperature.

Synthesis of the complexes

Synthesis of [Ru(dmb)$_2$(nfip)](PF$_6$)$_2$ (1)

A mixture of *cis*-[Ru(dmb)$_2$Cl$_2$]·2H$_2$O [28] (0.288 g, 0.50 mmol) and nfip (0.166 g, 0.50 mmol) [27] in ethylene glycol (20 mL) was refluxed under argon for 8 h to give a clear red solution. Upon cooling, a red precipitate was obtained by dropwise addition of saturated aqueous

Scheme 1 The synthetic route of ligand and complexes
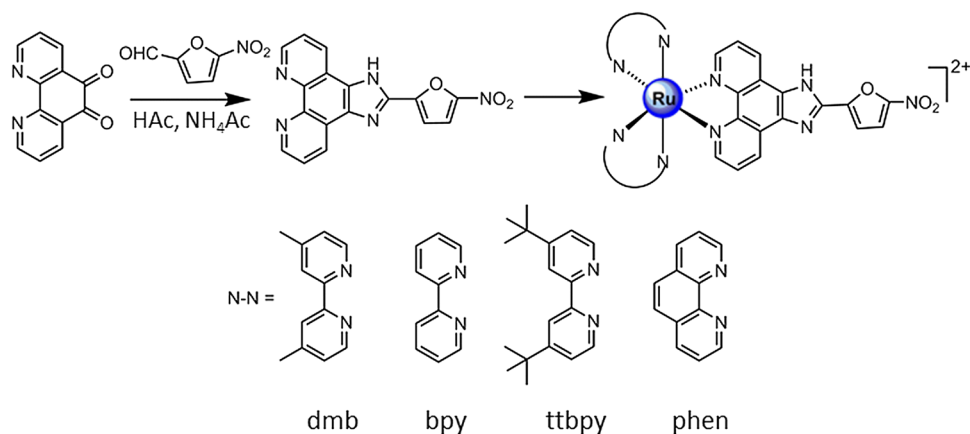
NH_4PF_6 solution. The crude product was purified by column chromatography on neutral alumina with a mixture of CH_3CN–toluene (1:1, v/v) as eluent. The red band was collected. The solvent was removed under reduced pressure, and a red powder was obtained. Yield: 70%. Anal. Calc for $C_{41}H_{33}N_9O_3F_{12}P_2Ru$: C, 45.09; H, 3.05; N, 11.55%. Found: C, 45.24; H, 3.13; N, 11.43%. IR (KBr, cm^{-1}): 3424 s, 2969 m, 1618 s, 1584 m, 1527 m, 1481 s, 1442 s, 1384 m, 1367 m, 1335 s, 1181 s, 1048w, 847 s, 726 s, 558 s. ^1H NMR: 8.88 (d, 2H, $J = 8.0$ Hz), 8.68 (d, 4H, $J = 8.0$ Hz), 7.84 (d, 4H, $J = 4.0$ Hz), 7.72 (dd, 2H, $J = 8.0$, $J = 8.5$ Hz), 7.67 (d, 2H, $J = 6.0$ Hz), 7.41 (dd, 4H, $J = 6.0$, $J = 6.5$ Hz), 7.31 (d, 1H, $J = 3.5$ Hz), 7.17 (d, 2H, $J = 5.5$ Hz), 1.91 (s, 6H), 1.64 (s, 6H). ^{13}C NMR (DMSO-d_6, 125 Hz): 156.43, 156.25, 150.80, 150.44, 149.43, 149.28, 147.74, 144.87, 129.78, 128.48, 128.43, 125.95, 125.39, 124.97, 124.92, 116.44, 110.22, 20.79, 20.72. ESI–MS (CH_3CN): m/z 946.0 ($[M–PF_6]^+$, 800.3 ($[M–2PF_6–H]^+$), 400.8 ($[M–2PF_6]^{2+}$).

Synthesis of [Ru(bpy)₂(nfip)](PF₆)₂ (2)

This complex was synthesized in a manner identical to complex **1**. Yield: 70%. Anal. Calc for $C_{37}H_{25}N_9O_3F_{12}P_2Ru$: C, 42.90; H, 2.43; N, 12.18%. Found: C, 42.82; H, 2.54; N, 12.42%. IR (KBr, cm^{-1}): 3425 s, 2967 m, 1604 m, 1466 m, 1444 s, 1394 m, 1365w, 1334w, 1179 m, 1049w, 844 s, 767 s, 559 s. ^1H NMR: 8.92 (d, 2H, $J = 8.0$ Hz), 8.84 (dd, 4H, $J = 8.0$, $J = 8.5$ Hz), 8.19 (t, 2H, $J = 7.0$ Hz), 8.08 (t, 2H, $J = 6.5$ Hz), 7.85 (dd, 4H, $J = 4.0$, $J = 5.0$ Hz), 7.73 (dd, 2H, $J = 5.0$, $J = 5.5$ Hz), 7.63 (d, 2H, $J = 5.5$ Hz), 7.57 (t, 2H, $J = 5.5$ Hz), 7.37 (t, 2H, $J = 6.0$ Hz), 7.32 (d, 2H, $J = 4.0$ Hz). ^{13}C NMR (DMSO-d_6, 125 Hz): 156.91, 156.67, 151.43, 151.37, 150.88, 147.87, 144.69, 137.87, 137.71, 136.23, 130.22, 127.88, 127.84, 125.99, 125.56, 124.45, 124.38, 116.45, 110.37. ESI–MS (CH_3CN): m/z 744.0 ($[M–2PF_6–H]^+$), 372.4 ($[M–2PF_6]^{2+}$).

Synthesis of [Ru(ttbpy)₂(nfip)](PF₆)₂ (3)

This complex was synthesized in a manner identical to that described for **1**, with $[Ru(ttbpy)_2Cl_2]·2H_2O$ [28] in place of $[Ru(dmb)_2Cl_2]·2H_2O$. Yield: 0.366 g, 72%. Anal. Calc for $C_{53}H_{57}N_9O_3F_{12}P_2Ru$: C, 50.50; H, 4.56; N, 10.01%. Found: C, 50.61; H, 4.34; N, 10.13%. IR (KBr, cm^{-1}): 3434 s, 2967 s, 1614 s, 1507w, 1482 m, 1415 m, 1384 m, 1345w, 1252 m, 1130 m, 1049 m, 841 s, 558 s. ^1H NMR: 8.92 (d, 2H, $J = 7.5$ Hz), 8.67 (d, 2H, $J = 6.5$ Hz), 8.83 (d, 2H, $J = 7.0$ Hz), 7.83 (d, 2H, $J = 4.0$ Hz), 7.79–7.74 (m, 3H), 7.69 (d, 2H, $J = 6.0$ Hz), 7.60 (dd, 2H, $J = 6.5$, $J = 6.0$ Hz), 7.48 (d, 2H, $J = 6.0$ Hz), 7.36 (dd, 2H, $J = 6.5$,

$J = 7.0$ Hz), 7.29 (d, 2H, $J = 8.5$ Hz), 1.42 (s, 18H), 1.31 (s, 18H). ^{13}C NMR (DMSO-d_6, 125 Hz): 161.73, 161.57, 156.66, 156.45, 150.76, 150.64, 147.46, 144.75, 138.78, 129.87, 126.17, 125.47, 124.79, 124.61, 121.79, 116.49, 110.08, 35.57, 35.44, 30.15, 30.03. ESI–MS (CH_3CN): m/z 968.4 ($[M–2PF_6–H]^+$), 484.7 ($[M–2PF_6]^{2+}$).

Synthesis of [Ru(phen)₂(nfip)](PF₆)₂ (4)

This complex was synthesized in a manner identical to that described for **1**, with $[Ru(phen)_2Cl_2]·2H_2O$ [28] in place of $[Ru(dmb)_2Cl_2]·2H_2O$. Yield: 72%. Anal. Calc for $C_{41}H_{25}N_9O_3F_{12}P_2Ru$: C, 45.43; H, 2.33; N, 11.64%. Found: C, 45.31; H, 2.47; N, 11.55%. IR (KBr, cm^{-1}): 3386 s, 2970 m, 1629 m, 1582 s, 1524 m, 1480 s, 1442 s, 1426 m, 1364 m, 1331 s, 1253w, 1179 s, 1082 m, 1025 s, 842 s, 721 s, 558 s. ^1H NMR: 8.84 (d, 2H, $J = 8.0$ Hz), 8.74 (dd, 4H, $J = 8.5$, $J = 8.0$ Hz), 8.36 (s, 4H), 8.13 (d, 2H, $J = 5.0$ Hz), 8.09 (d, 2H, $J = 5.0$ Hz), 7.83 (d, 1H, $J = 8.0$ Hz), 7.78–7.73 (m, 7H), 7.57 (dd, 2H, $J = 8.0$, $J = 8.5$ Hz), 7.29 (d, 1H, $J = 4.0$ Hz). ^{13}C NMR (DMSO-d_6, 125 Hz): 152.65, 150.65, 147.98, 147.39, 144.91, 136.64, 130.48, 130.44, 130.05, 128.11, 128.06, 126.33, 125.23, 116.58, 109.87. ESI–MS (CH_3CN): m/z 792.1 ($[M–2PF_6–H]^+$), 396.4 ($[M–2PF_6]^{2+}$).

Synthesis of [Ru(dmp)₂(nfip)](PF₆)₂ (5)

This complex was synthesized in a manner identical to that described for **1**, with $[Ru(dmp)_2Cl_2]·2H_2O$ [29] in place of $[Ru(dmb)_2Cl_2]·2H_2O$. Yield: 71%. Anal. Calc for $C_{45}H_{33}N_9O_3F_{12}P_2Ru$: C, 47.41; H, 2.92; N, 11.06%. Found: C, 47.58; H, 3.07; N, 10.97%. IR (KBr, cm^{-1}): 3411 s, 2969 m, 1627 m, 1587 s, 1527 m, 1499 s, 1441 s, 1392 m, 1365 m, 1333 s, 1180 s, 1130w, 1084 s, 1047 s, 845 s, 728 m, 557 s. ^1H NMR: 8.89 (d, 2H, $J = 8.0$ Hz), 8.76 (d, 2H, $J = 8.5$ Hz), 8.41 (dd, 4H, $J = 8.5$, $J = 8.0$ Hz), 8.22 (d, 2H, $J = 8.5$ Hz), 7.95 (d, 2H, $J = 8.5$ Hz), 7.80 (d, 2H, $J = 4.0$ Hz), 7.38–7.32 (m, 4H), 7.27 (d, 1H, $J = 4.0$ Hz), 7.15 (dd, 2H, $J = 5.0$, $J = 5.5$ Hz), 1.93 (s, 6H), 1.71 (s, 6H). ^{13}C NMR (DMSO-d_6, 125 Hz): 167.85, 166.21, 150.76, 149.04, 148.66, 148.02, 145.25, 137.96, 136.66, 130.36, 129.53, 129.47, 127.50, 127.33, 127.16, 126.49, 125.49, 124.41, 116.41, 110.14, 25.42, 24.57. ESI–MS (CH_3CN): m/z 848.3 ($[M–2PF_6–H]^+$), 424.0 ($[M–2PF_6]^{2+}$).

In vitro cytotoxicity assay

MTT assay procedures were used [30]. Cells were placed in 96-well microassay culture plates (8×10^3 cells per well) and grown overnight at 37 °C in a 5% CO_2 incubator. The tested complex was dissolved in DMSO and then added to the wells to achieve final concentrations ranging from 10^{-6} to 10^{-4} M. Control wells were prepared by addition of culture medium

(100 μL). The plates were incubated at 37 °C in a 5% CO_2 incubator for 48 h. Upon completion of the incubation, stock MTT dye solution (20 μL, 5 mg mL^{-1}) was added to each well. After 4 h, buffer (100 μL) containing dimethylformamide (50%) and sodium dodecyl sulfate (20%) was added to solubilize the MTT formazan. The optical density of each well was measured with a microplate spectrophotometer at a wavelength of 490 nm. The IC_{50} values were determined by plotting the percentage of viable cells versus concentration on a logarithmic graph and reading of the concentration at which 50% of cells remained viable relative to the control. Each experiment was repeated at least three times to obtain mean values.

Apoptosis assay by AO/EB staining method

SGC-7901 cells were seeded onto chamber slides in six-well plates at a density of 2×10^5 cells per well and incubated for 24 h. The cells were cultured in RPMI 1640 supplemented with 10% of fetal bovine serum (FBS) and incubated at 37 °C in 5% CO_2. The medium was removed and replaced with medium (final DMSO concentration, 0.05% v/v) containing the complexes (6.25 μM) for 24 h. The medium was removed again, and the cells were washed with ice-cold phosphate buffer saline (PBS) and fixed with formalin (4%, w/v). Cell nuclei were counterstained with acridine orange (AO) and ethidium bromide (EB) (AO: 100 μg mL^{-1}, EB: 100 μg mL^{-1}) for 10 min. The cells were observed and imaged with a fluorescence microscope (Nikon, Yokohama, Japan) with excitation at 350 nm and emission at 460 nm.

Comet assay

DNA damage was investigated by means of comet assay. SGC-7901 cells in culture medium were incubated with 6.25 μM of complexes **1–4** for 24 h at 37 °C. The control cells were also incubated at the same time. The cells were harvested by a trypsinization process at 24 h. A total of 100 μL of 0.5% normal agarose in PBS was dropped gently onto a fully frosted microslide, covered immediately with a coverslip and then kept at 4 °C for 10 min. The coverslip was removed after the gel had set. 50 μL of the cell suspension (200 cells per μL) was mixed with 50 μL of 1% low melting agarose preserved at 37 °C. A total of 100 μL of this mixture was applied quickly on top of the gel, coated over the microslide, covered immediately with a coverslip and then kept at 4 °C for 10 min. The coverslip was again removed after the gel had set. A third coating of 50 μL of 0.5% low melting agarose was placed on the gel and allowed to set at 4 °C for 15 min. After solidification of the agarose, the coverslips were removed, and the slides were immersed in an ice-cold lysis solution (2.5 M NaCl, 100 mM EDTA, 10 mM Tris, 90 mM sodium sarcosinate, NaOH, pH 10, 1% Triton

X-100 and 10% DMSO) and placed in a refrigerator at 4 °C for 2 h. All of the above operations were performed under low lighting conditions to avoid additional DNA damage. The slides, after removal from the lysis solution, were placed horizontally in an electrophoresis chamber. The reservoirs were filled with an electrophoresis buffer (300 mM NaOH, 1.2 mM EDTA) until the slides were just immersed in it, and the DNA was allowed to unwind for 30 min in electrophoresis solution. Then the electrophoresis was carried out at 25 V and 300 mA for 20 min. After electrophoresis, the slides were removed and washed thrice in a neutralization buffer (400 mM Tris, HCl, pH 7.5). Cells were stained with 20 μL of EB (20 μg mL^{-1}) in the dark for 20 min. The slides were washed in chilled distilled water for 10 min to neutralize the excess alkali, air-dried and scored for comets by fluorescence microscopy.

Location of the complexes at the lysosomes

SGC-7901 cells were placed in 12-well microassay culture plates (4×10^4 cells per well) and grown overnight at 37 °C in a 5% CO_2 incubator. 6.25 μM of the complexes were added to the wells at 37 °C in a 5% CO_2 incubator for 6 h and further co-incubated with LysoTracker Green (150 nM) at 37 °C for 0.5 h. Upon completion of the incubation, the wells were washed three times with ice-cold PBS. After discarding the culture medium, the cells were imaged under a fluorescence microscope.

Detection of lysosome membrane permeabilization

SGC-7901 cells were placed in 12-well microassay culture plates (4×10^4 cells per well) and grown overnight at 37 °C in a 5% CO_2 incubator. 6.25 μM of the complex was added to the wells at 37 °C in a 5% CO_2 incubator for 24 h and further co-incubated with AO (1 μg/mL) at 37 °C for 0.5 h. Upon completion of the incubation, the wells were washed three times with ice-cold PBS. After discarding the culture medium, the cells were imaged under a fluorescence microscope.

Location assay of the complex in the mitochondria

SGC-7901 cells were placed in 12-well microassay culture plates (4×10^4 cells per well) and grown overnight at 37 °C in a 5% CO_2 incubator. 6.25 μM of the complex was added to the wells at 37 °C in a 5% CO_2 incubator for 12 h and further co-incubated with MitoTracker ® Deep Green FM (150 nM) at 37 °C for 0.5 h. Upon completion of the incubation, the wells were washed three times with ice-cold PBS. After discarding the culture medium, the cells were imaged under a fluorescence microscope.

Mitochondrial membrane potential assay

SGC-7901 cells were treated for 24 h with different concentrations of the complex in 12-well plates and were then washed three times with cold PBS. The cells were detached with trypsin–EDTA solution. The collected cells were incubated for 20 min with 1 µg mL^{-1} of JC-1 (5,5′,6,6′-tetrachloro-1,1′,3,3′-tetraethylimidacarbocyanine iodide) in culture medium at 37 °C. The cells were then immediately centrifuged to remove the supernatant. The cell pellets were suspended in PBS. The ratio of red/green fluorescence intensity was determined by flow cytometry.

Reactive oxygen species (ROS) detection

SGC-7901 cells were seeded into six-well plates (Costar, Corning Corp, New York) at a density of 2×10^5 cells per well and incubated for 24 h. The cells were cultured in RPMI 1640 medium supplemented with 10% FBS and incubated at 37 °C in 5% CO_2. The medium was removed and replaced with medium (final DMSO concentration, 0.05% v/v) containing different concentrations of the complex for 24 h. The medium was removed again. The fluorescent dye 2′,7′-dichlorodihydrofluorescein diacetate (DCHF-DA, 10 µM) was added to the medium to cover the cells. The treated cells were then washed with cold PBS–EDTA twice and collected by trypsinization and centrifugation at 1500 rpm for 5 min, and the cell pellets were suspended in PBS-EDTA. The DCF fluorescence intensity was determined by flow cytometry.

Cell cycle arrest by flow cytometry

SGC-7901 cells were seeded into six-well plates (Costar, Corning Corp, New York) at a density of 2×10^5 cells per well and incubated for 24 h. The cells were cultured in RPMI 1640 medium supplemented with 10% FBS and incubated at 37 °C in 5% CO_2. The medium was removed and replaced with medium (final DMSO concentration, 0.05% v/v) containing the complex (12.5 µM). After incubation for 24 h, the cell layer was trypsinized and washed with cold PBS and fixed with 70% ethanol. 20 µL of RNAse (0.2 mg mL^{-1}) and 20 µL of propidium iodide (0.02 mg mL^{-1}) were added to the cell suspensions, which were then incubated at 37 °C for 30 min. Then the samples were analyzed with a FACSCalibur flow cytometer. The number of cells analyzed for each sample was 10 000 [31].

The percentage of apoptotic cells assay by flow cytometry

After chemical treatment, 1×10^6 SGC-7901 cells were harvested, washed with PBS, fixed with 70% ethanol and finally maintained at 4 °C for at least 12 h. The pellets were stained with a fluorescent probe solution containing 50 µg/mL PI and 1 mg/mL Annexin V in PBS on ice in the dark for 15 min. The fluorescence emission was measured at 530 nm (excitation at 488 nm) with a FACSCalibur flow cytometer (Beckman Dickinson & Co., Franklin Lakes, NJ). A minimum of 10,000 cells were analyzed per sample.

Autophagy induced by the complexes

SGC-7901 cells were seeded onto chamber slides in 12-well plates and incubated for 24 h. The cells were cultured in RPMI 1640 medium supplemented with 10% FBS and incubated at 37 °C in 5% CO_2. The medium was removed and replaced with medium (final DMSO concentration, 0.05% v/v) containing different concentrations of the complex for 24 h. The medium was removed again, and the cells were washed with ice-cold PBS twice. Then the cells were stained with MDC (monodansylcadaverine) solution (50 µM) for 10 min and washed with PBS twice. The cells were observed and imaged under a fluorescence microscope. The effect of the complex on the expression of LC3 and beclin-1 proteins was assayed by Western blot.

Matrigel invasion assays

A BD Matrigel invasion chamber was used to investigate cell invasion according to the manufacturer's instructions. SGC-7901 cells (4×10^4) in serum-free medium containing different concentrations of the complex were seeded into the top chamber of the two-chamber Matrigel system. RPMI 1640 medium (20% FBS) was added into the lower chamber. The cells were allowed to invade for 24 h. After incubation, noninvading cells were removed from the upper surface and cells on the lower surface were fixed with 4% paraformaldehyde and stained with 0.1% crystal violet. The membranes were photographed, and the invading cells were counted under a light microscope. The mean values from three independent assays were calculated.

Measurement of intracellular Ca^{2+}

SGC-7901 cells were seeded into chamber slides in 12-well plates and incubated for 24 h. The cells were cultured in RPMI 1640 medium supplemented with 10% FBS and incubated at 37 °C in 5% CO_2. The medium was removed and replaced with medium (final DMSO concentration, 0.05% v/v) containing 6.25 µM of the complexes for 24 h. The medium was removed again, and the cells were washed with PBS twice. Then the cells were stained with Fluo-3AM (Molecular Probes, Eugene, OR) (2.5 µM) for 30 min and washed with PBS twice. After this, the cells were stained with Hoechst (10 µg mL^{-1}) for 30 min and washed with

PBS twice. The cells were imaged and analyzed under the Molecular Devices.

Release of cytochrome c

SGC-7901 cells were seeded onto chamber slides in 12-well plates and incubated for 24 h. The cells were cultured in RPMI 1640 medium supplemented with 10% FBS and incubated at 37 °C in 5% CO_2. The medium was removed and replaced with medium (final DMSO concentration, 0.05% v/v) containing 6.25 µM of the complexes for 24 h. The medium was removed again, and the cells were washed with PBS twice. Then cells were fixed with stationary liquid overnight at 4 °C. Then the cells were incubated with confining liquid for 1 h and washed with PBST for three times. Next, the cells were incubated with primary antibody of human cytochrome c for 24 h. After washing, incubation with fluorescein-conjugated anti-rabbit secondary antibody and mounting were done with paramounting media containing DAPI, scored and analyzed under the Molecular Devices.

Expression of caspases and Bcl-2 family proteins

SGC-7901 cells were seeded into 3.5-cm dishes for 24 h and incubated with 12.5 µM of the complex in the presence of 10% FBS. The cells were harvested in lysis buffer. After sonication, the samples were centrifuged for 20 min at 13 000 g. The protein concentration of the supernatant was determined by BCA (bicinchoninic acid) assay. Sodium dodecyl sulfate–polyacrylamide gel electrophoresis was performed by loading equal amounts of protein per lane. The gels were then transferred to poly(vinylidene difluoride) membranes (Millipore) and blocked with 5% nonfat milk in TBST (20 mM Tris-HCl, 150 mM NaCl, 0.05% Tween 20, pH 8.0) buffer for 1 h. Then the membranes were incubated with primary antibodies at 1:5000 dilutions in 5% nonfat milk overnight at 4 °C and washed four times with TBST for a total of 30 min. After this, the membranes were incubated with secondary antibodies conjugated with horseradish peroxidase at 1:5000 dilution for 1 h at room temperature and then washed four times with TBST. The blots were visualized using Amersham ECL Plus Western blotting detection reagents according to the manufacturer's instructions. To assess the presence of comparable amounts of protein in each lane, the membranes were stripped finally to detect the β-actin. The gray values were calculated using BANDSCAN.

Data analysis

All data are expressed as mean ± SD. Statistical significance was evaluated using *t* tests. Differences were considered to be significant when the *P value was less than 0.05.

Results and discussion

Synthesis and characterization

The synthesis of the proligand and its complexes is shown in Scheme 1. The proligand nfip was prepared through condensation of 1,10-phenanthroline-5,6-dione with 5-nitrofuran-2-carbaldehyde according to the literature [27]. The corresponding ruthenium(II) mixed-ligand complexes were synthesized by direct reaction of nfip with the appropriate precursor complexes in ethylene glycol. The desired ruthenium(II) complexes were isolated as the hexafluorophosphate and purified by column chromatography. The UV–Vis and luminescence spectra of the complexes 1–5 are shown in Fig. S1 (supporting information). The UV–Vis spectra (a) of the five Ru(II) complexes are characterized by intense π–π* ligand transitions in the UV and metal-to ligand charge transfer (MLCT) transition in the visible region. The absorption spectra of complexes 1–5 mainly consist of two well-resolved bands in the range 200–600 nm. The lowest energy band at 475 nm for 1, 465 nm for 2, 474 nm for 3, 464 nm for 4 and 477 nm for 5 is assigned to the metal-to-ligand charge transfer (MLCT) transition, and the high-energy bands below 300 nm are attributed to intraligand (IL) p–p* transitions. The complexes 1–4 are luminescent at room temperature (b), with a maximum appearing at 623 nm for 1, 600 nm for 2, 608 nm for 3 and 617 nm for 4, respectively, whereas complex 5 is not luminescent at room temperature. In the ESI–MS spectra for the complexes, all of the expected signals $[M-PF_6]^+$, $[M-2PF_6-H]^+$ and $[M-2PF_6]^{2+}$ were observed. The measured molecular weights were consistent with the expected values. In the IR spectra of the complexes, the peaks at 3424 cm^{-1} for 1, 3434 cm^{-1} for 3, 3386 cm^{-1} for 4 and 3411 cm^{-1} for 5 are assigned to the stretch vibration of the NO_2 group. In the ^{13}C NMR spectra for the complexes (Fig. S2, supporting information), the peaks of 20.79 and 20.72 for 1, 35.57, 35.44, 30.15 and 30.03 for 3, 25.42 and 24.57 for 5 are attributed to the characteristic of –CH_3 group.

In vitro cytotoxicity

In order to study the antitumor potential of the complexes 1–5, the inhibition of cell growth in Eca-109, HepG2, A549, HeLa, SGC-7901 and normal LO2 was detected by MTT assays. Cisplatin was used as a positive control. The IC_{50} values of the tested compounds are shown in Table 1. Surprisingly, complexes 2–5 have no cytotoxic effect on the cell growth of normal LO2, but cisplatin has a strong toxicity to normal cells (9.2 ± 1.4 µM). Complexes 1–4 show no cytotoxicity toward HepG2 and A549 cells, and complex 5 displays no cytotoxic effect on the cell growth in SGC-7901,

Table 1 IC$_{50}$ values of the complexes against selected cancer cells

Complexes	SGC-7901	Eca-109	HepG2	A549	HeLa	LO2
1	12.4 ± 1.4	74.1 ± 5.5	> 200	> 200	> 200	69.2 ± 4.4
2	6.7 ± 1.6	> 200	> 200	> 200	> 200	> 200
3	1.3 ± 0.5	> 200	> 200	> 200	> 200	> 200
4	1.1 ± 0.4	> 200	> 200	> 200	23.1 ± 2.8	> 200
5	> 200	> 200	> 200	18.3 ± 2.4	2.1 ± 0.6	> 200
Cisplatin	3.8 ± 0.5	–	11.9 ± 1.5	7.7 ± 1.3	7.0 ± 1.0	9.1 ± 1.4

Eca-109 and HepG2 cells. Comparing the IC$_{50}$ values, complexes **3** and **4** show higher anticancer activity against SGC-7901 than cisplatin, and complex **5** displays higher cytotoxic effect toward HeLa cells than cisplatin under the same conditions. These results demonstrate that complexes **1–4** significantly inhibit the cell growth in human gastric cancer SGC-7901 cells in a dose-dependent manner. Because complex **5** has no cytotoxic activity against SGC-7901, in the following experiments, complexes **1–4** were used to detect the anticancer activity against SGC-7901 cells.

Measurement of DNA damage by comet assay

DNA fragmentation is a characteristic of apoptosis and mitosis mutations [32]. In order to evaluate the effect of the complexes on DNA damage, the DNA damage was detected using single cell gel electrophoresis (comet assay). As shown in Fig. 1, the cell nuclei in control (a) appear round. After the treatment of SGC-7901 cells with 6.25 μM of complexes **1** (b), **2** (c), **3** (d) and **4** (e) for 24 h, complexes **1–4** cause a marked increase in comet tail lengths compared with those of the control, which confirms their ability to cleave cellular DNA, providing further evidence of apoptosis.

AO/EB staining for apoptotic cells

Apoptosis is usually considered a unique pattern of gene-controlled cell autonomously ordered death [33]. In general, apoptotic cells can undergo morphological changes such as cell shrinkage, nuclear condensation, DNA fragmentation and formation of apoptotic bodies. The DNA damage demonstrates that the complexes can cause apoptosis. In order to further observe the apoptotic effect induced by the complexes, the apoptotic assay was performed by acridine orange (AO) and ethidium bromide (EB) staining method. It is well known that AO permeates the intact cells and stains the nuclei green, whereas EB penetrates only membrane disintegrated cells and stains the nucleus red. It can be observed from Fig. 2A that the cells in the control (a) were stained green and maintained intact cell morphology. When the SGC-7901 cells were incubated with 6.25 μM complexes **1** (b), **2** (c), **3** (d) and **4** (e) for 24 h, the morphology of the cells obviously changed, and the cells are shrunk and rounded. Therefore, complexes **1–4** can induce apoptosis in SGC-7901 cells. To compare the apoptotic efficiency of the complexes against SGC-7901 cells, the apoptotic percentage in the cells was determined by flow cytometry. As shown in Fig. 2B, the early apoptotic percentage (Q3) in the control group (a) is 0.94%. After treatment of SGC-7901 cells with 6.25 μM of the complexes for 24 h, the percentages of early apoptotic SGC-7901 cells were 5.89% for complex **1** (b), 3.36% for complex **2** (c), 5.93% for complex **3** (d) and 8.26% for complex **4** (e), respectively. The apoptotic effect follows the order of **4 > 3 > 1 > 2**. Complex **4** shows the highest apoptotic efficiency among the four complexes. The results indicate that complexes can effectively induce apoptosis in SGC-7901 cells.

Location of the complexes in the lysosomes and lysosome membrane permeability studies

Lysosomes are involved in cell death and cell signaling [34]. In order to evaluate whether the complexes act on lysosomes, LysoTracker Green as a fluorescent probe was used
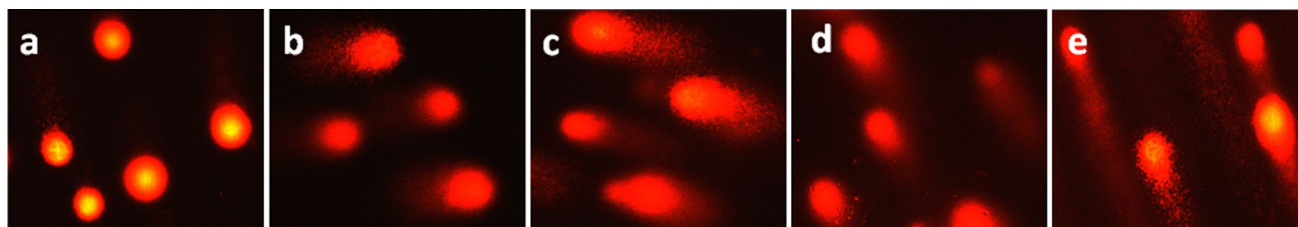

Fig. 1 Comet assays of SGC-7901 cells (**a**) exposure to 6.25 μM of complexes **1** (**b**), **2** (**c**), **3** (**d**) and **4** (**e**) for 24 h
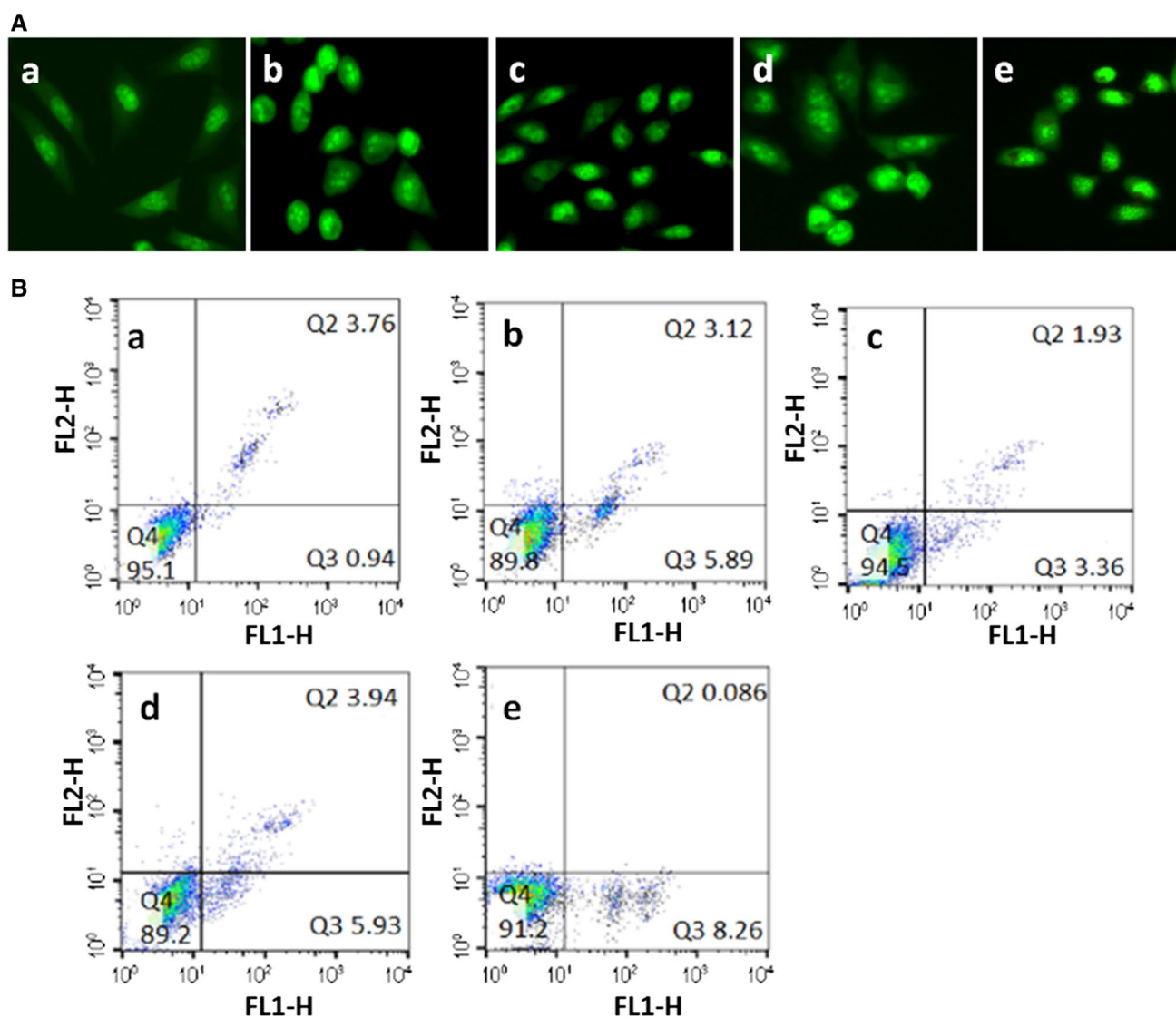
Fig. 2 Apoptosis was assayed with AO/EB (**A**) and Annex V/PI (**B**) staining SGC-7901 cell (a) induced by 6.25 μM of complexes **1** (b), **2** (c), **3** (d) and **4** (e) for 24 h

to detect the colocalization of the complexes in intercellular lysosomes. As shown in Fig. 3A, the lysosomes stained with LysoTracker Green show bright green. After SGC-7901 cells were exposed to 6.25 μM of complexes **1–4** for 6 h, the Ru(II) complexes **1–4** emit red fluorescence. The merge displays yellow which suggests the complete overlap of the red and green, indicating that the complexes locate at the intercellular lysosomes. The lysosomes contain many different acid hydrolases. The change of lysosome membrane permeabilization (LMP) can release the lysosomal constituents, which further trigger cell death. LMP was assessed by the AO relocation method. AO is weakly alkaline and can accumulate in acidic lysosomal compartments. AO is also a metachromatic fluorescent dye; it exhibits red fluorescence at high concentrations at acidic pH (in intact lysosomes), but

green fluorescence at low concentrations (when lysosomal contents diffuse into the cytosol) [35]. As shown in Fig. 3B, a number of obvious red fluorescent points were observed in the control (a). After SGC-7901 cells were exposed to 6.25 μM of complexes **1–4** (b–e) for 24 h, the red fluorescence decreased significantly. Thus, the complexes can induce lysosomal membrane permeabilization.

Studies of the location of complexes in the mitochondria

Mitochondria are potential sources of ROS produced by cells [36]. Mitochondrial changes, including the loss of mitochondrial membrane potential, are key events that occur during drug-induced apoptosis [37]. Therefore, we conducted a
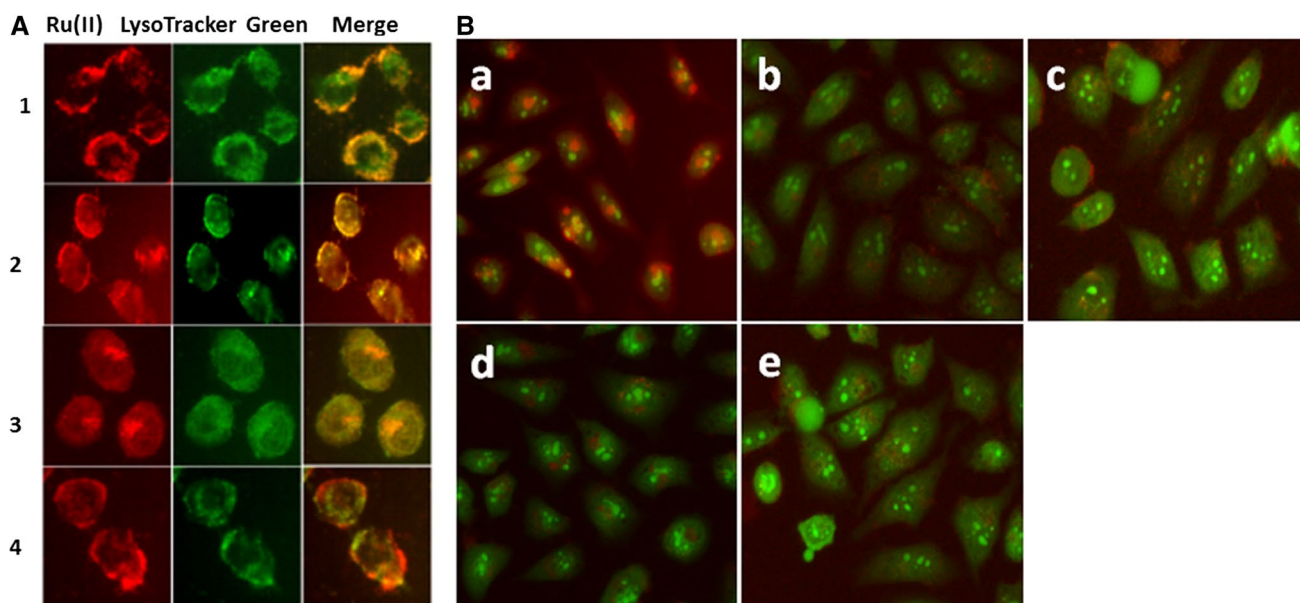
Fig. 3 **A** Location assay of **1**–**4** in the lysosomes after SGC-7901 cells were exposed to 6.25 µM of the complexes for 6 h and the cells were stained with LysoTracker Green. **B** The permeability of lysosomes induced by 6.25 µM of the complexes treated with SGC-7901 cells for 24 h and the cells were stained with AO. (Color figure online)

series of experiments to explore the location of the complexes in the mitochondria and the changes of mitochondrial membrane potential. The studies of the complexes on the location of lysosomes illustrate that the complexes locate at the lysosomes during the treatment of SGC-7901 cells with the complexes for 6 h. In the meantime, we also evaluated the location of the complexes at the mitochondria. As shown in Fig. 4A, the mitochondria were stained green, the complexes emit weak red fluorescence, which indicates that only small amounts of the complexes enter into the mitochondria. However, after SGC-7901 cells were treated with 6.25 µM of the complexes for 8 h (Fig. 4B), the green (mitochondria) and red (the complexes) can overlap, indicating that the complexes enter into the mitochondria. Thus, we infer that the complexes enter into the lysosomes and cause lysosomal membrane permeability; then, the complexes enter into the mitochondria.

The changes of mitochondrial membrane potential

JC-1 was used to detect the changes of mitochondrial membrane potential. It is well known that JC-1 accumulates in healthy mitochondria to form red fluorescent aggregates. After depolarization, the aggregates decompose and lose red fluorescence, and the green fluorescence of JC-1 monomer is dominant. As shown in Fig. 4C, in the control (a), JC-1 emits red fluorescence corresponding to high mitochondrial membrane potential. After SGC-7901 cells were incubated with cccp (b, positive control) and 6.25 µM of complexes **1** (c), **2** (d), **3** (e) and **4** (f) for 24 h, JC-1 emits bright green

fluorescence, which corresponds to low mitochondrial membrane potential. The changes from red fluorescence to green fluorescence indicate a decrease in mitochondrial membrane potential. To further study the extent of changes of mitochondrial membrane potential induced by complexes **1**–**4**, the ratio of the red/green fluorescent intensity was determined by flow cytometry. As shown in Fig. 4D, the red/green ratio of the control group (a) is 3.19. When SGC-7901 cells were exposed to 6.25 µM of complexes **1**–**4** for 24 h, the ratios of red/green fluorescence were 2.07, 2.11, 1.79 and 1.73, respectively. The decrease in the ratio of red/green fluorescence demonstrates that the complexes induce a reduction of mitochondrial membrane potential. To evaluate the effect of ROS on the changes of mitochondrial membrane potential, the ratio of red/green fluorescent intensity was also studied. In the presence of NAC (NAC can inhibit to produce ROS), the ratios of red/green are 2.45 for **1** + NAC) and 2.05 for **4** + NAC, respectively. Obviously, in the presence of NAC, complexes **1** and **4** induce less decrease in the mitochondrial membrane potential. These results indicate that the complexes can induce a decrease in the mitochondrial membrane potential, and high ROS levels can induce larger changes of the mitochondrial membrane potential than those of low ROS levels.

Detection of intracellular reactive oxygen species, superoxide anion radical and nitric oxide

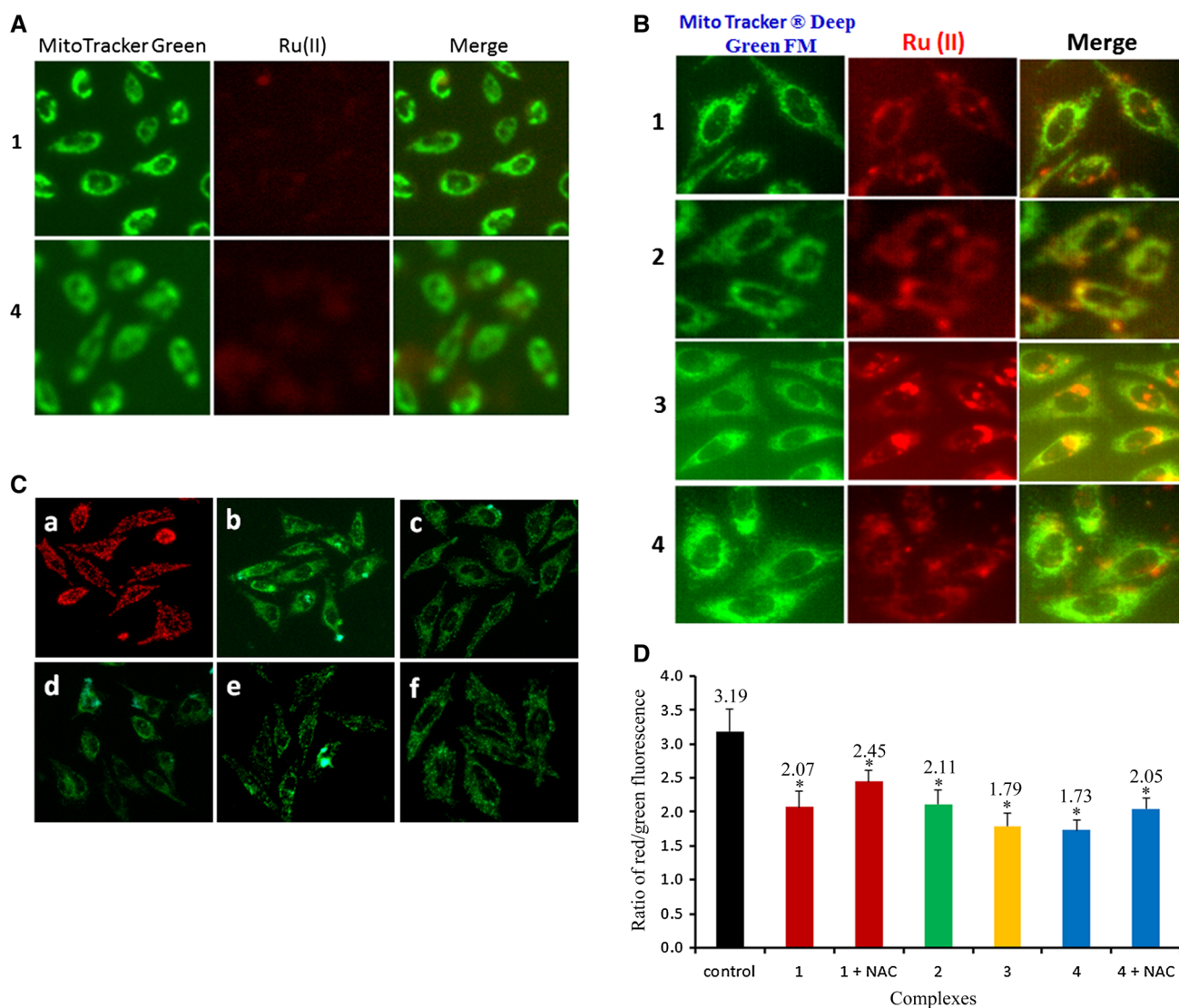ROS plays an important role in the nosogenesis of various human diseases [38], and apoptosis can be caused by

Fig. 4 Location assay of the complexes in the mitochondria after SGC-7901 cells were incubated with 6.25 μM of the complexes for 6 (**A**) and 8 h (**B**). **C** The mitochondrial membrane potential was determined under fluorescent microscope after SGC-7901 cells (a) were treated with complexes **1** (b), **2** (c), **3** (d) and **4** (e) for 24 h. **D** The ratio of red/green fluorescence intensity was determined by flow cytometry, while SGC-7901 cells were treated with 6.25 μM complexes **1**–**4** in the presence or absence of NAC for 24 h. *$P < 0.05$ represents significant differences compared with control

increasing intracellular ROS levels [39]. In the assay of intracellular ROS levels, 2′,7′-dichlorodihydrofluorescein diacetate (DCFH–DA) dye was used as a fluorescent probe. DCFH-DA is nonfluorescent and can be hydrolyzed by intracellular enzymes to produce DCFH. In the presence of ROS, this dye is changed into a highly fluorescent compound (2′,7′-dichlorofluorescein, DCF). As shown in Fig. 5A, no obvious fluorescent points are observed in the control group (a). After SGC-7901 cells were exposed to Rosup (b, positive control) and 6.25 μM of complexes **1** (c), **2** (d), **3** (e) and **4** (f) for 24 h, bright green fluorescent points are found. The findings show that the complexes can enhance intracellular ROS levels. In order to further compare the effect of the

complexes on intracellular ROS, ROS levels were measured by flow cytometry. As shown in Fig. 5B, after the treatment of SGC-7901 with 6.25 μM complexes **1** (b), **1** + NAC (c), **2** (d), **3** (e), **4** (f) and **4** + NAC (g) for 24 h, the fluorescent intensities of DCF increased by 2.46, 1.75, 1.85, 3.67, 5.26 and 4.20 times than those in the control (a), respectively. Complex **4** has the strongest ability to increase intracellular ROS levels. Furthermore, NAC inhibits production of ROS. In addition, the relationship between NAC and cell viability was also investigated. As shown in Fig. S1 (supporting information), in the presence of NAC, the cell viability increases compared to those in the absence of NAC for complexes
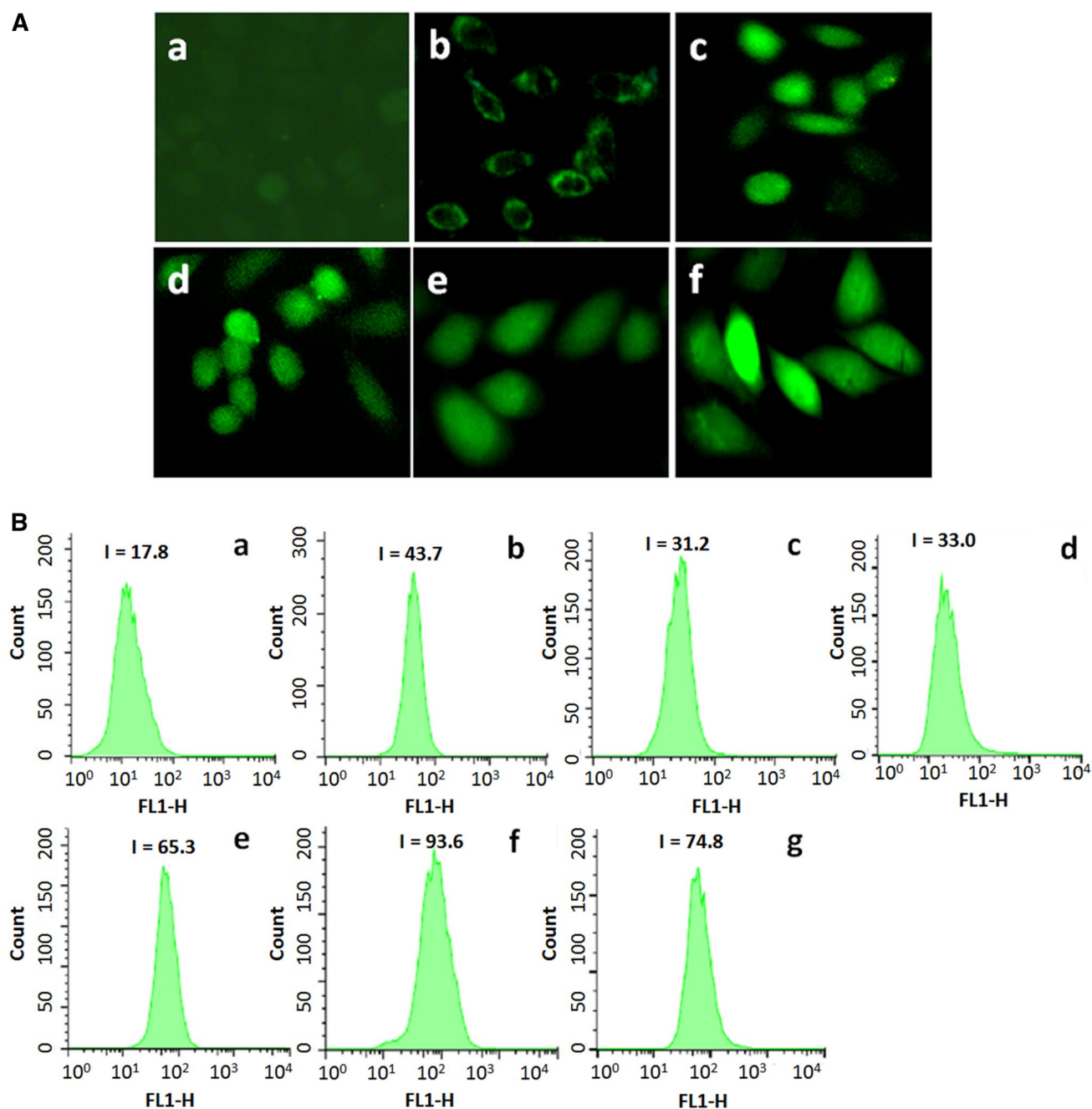
Fig. 5 A The intracellular ROS levels were assayed after SGC-7901 cells (a) were exposed to Rosup (b, positive control) and 6.25 μM of complexes **1** (c), **2** (d), **3** (e) and **4** (f) for 24 h. **B** DCF fluorescent intensity was determined by flow cytometry after SGC-7901 cells (a) were treated by 6.25 μM of complexes **1** (b), **1**+NAC (c), **2** (d), **3** (e) and **4** (f), **4**+NAC (g) for 24 h. **C** The intracellular superoxide anion levels were assayed after SGC-7901 cells (a) were exposed to 6.25 μM of complexes **1** (b), **2** (c), **3** (d) and **4** (e) for 24 h. **D** DHE fluorescent intensity was determined after SGC-7901 cells (a) were treated by 3.13 and 6.25 μM of complexes **1–4** for 24 h. **E** The intracellular NO levels were assayed after SGC-7901 cells (a) were exposed to 6.25 μM of complexes **1** (b), **2** (c), **3** (d) and **4** (e) for 24 h. **F** DAF-FMDA fluorescent intensity was determined after SGC-7901 cells (a) were treated by 3.13 and 6.25 μM of complexes **1–4** for 24 h. *$P < 0.05$ represents significant differences compared with control

1–4. The data suggest that ROS levels induce a decrease in cell viability.

ROS consists of many primary reactive oxygen species, including superoxide anion (O_2^-), hydrogen peroxide (H_2O_2) and singlet oxygen ($^1O_2$), hydroxyl radical (·OH) and NO [40–43]. Superoxide anion plays an important role in tumor cell damage. In the assay of reactive oxygen species, we found that the intracellular ROS levels increased
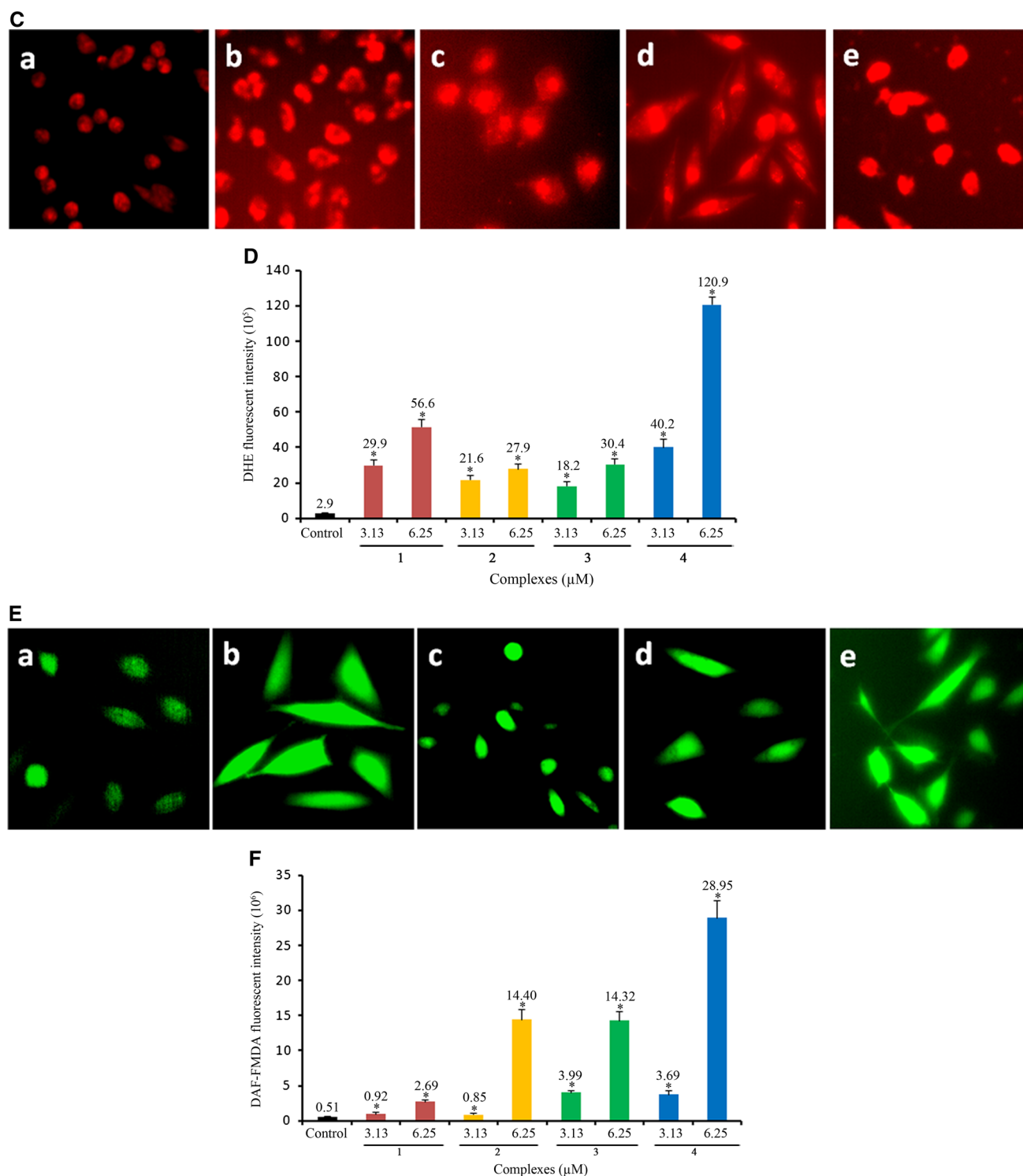
C

D

E

F

Fig. 5 (continued)

significantly. In order to further explore whether the levels of intracellular superoxide anion change, we used DHE as a fluorescent probe. DHE is nonfluorescent and can be oxidized by ROS to ethidium, which intercalates with DNA and stains nuclei bright red fluorescence. As shown in Fig. 5C, comparing with the control (a), the treatment of SGC-7901 cells with complexes **1** (b), **2** (c), **3** (d) and **4** (e) led to a significant increase in the red fluorescent points. The
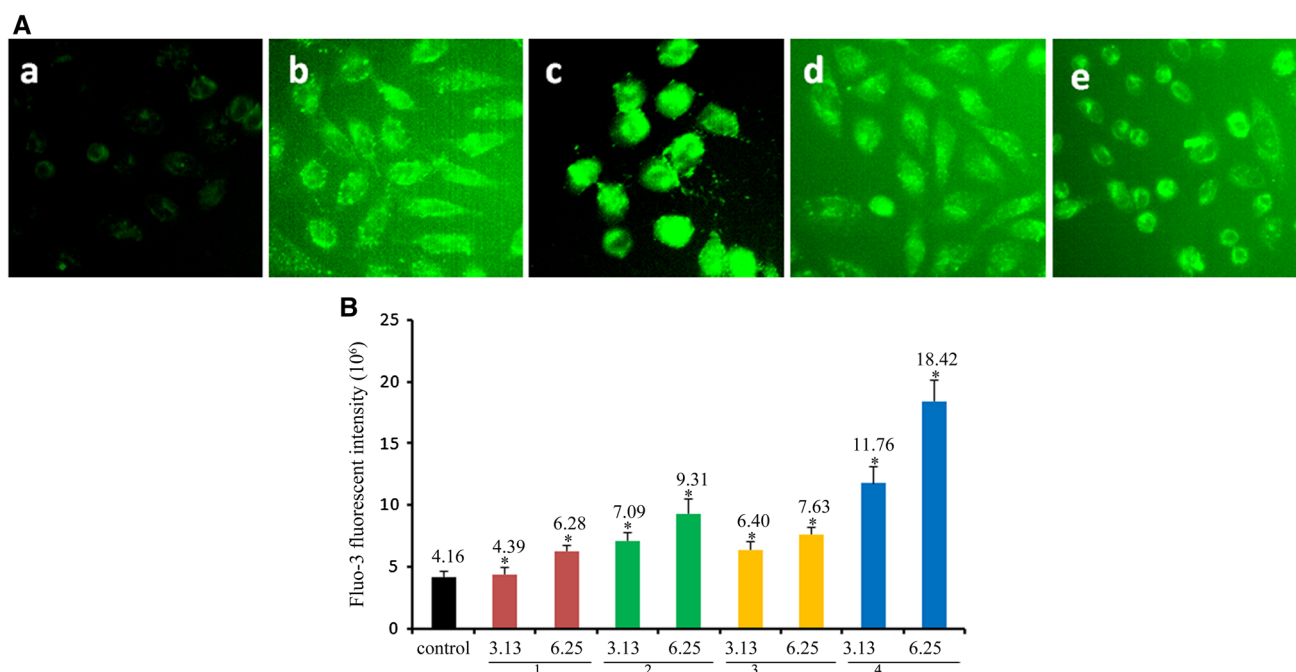
Fig. 6 A Intracellular Ca^{2+} levels were assayed after SGC-7901 cells (a) were exposed to 6.25 μM of complexes **1** (b), **2** (c), **3** (d) and **4** (e) for 24 h. **B** The integrated fluorescent intensity/cell was determined after SGC-7901 cells were treated with different concentration of complexes **1–4** for 24 h. *$P < 0.05$ represents significant differences compared with control

corresponding red fluorescence intensity was determined and is shown in Fig. 5D; the complexes **1–4** can enhance the DHE red fluorescence intensity in a concentration-dependent manner. Nitric oxide can induce apoptosis and necrosis [44], and NO can react rapidly with superoxide radicals to form peroxynitrite [45]. The intracellular NO levels were assayed using DAF-FM DA as a fluorescent probe. As shown in Fig. 5E, after the treatment of SGC-7901 cells with 6.25 μM of complexes **1** (b), **2** (c), **3** (d) and **4** (e) for 24 h, more bright green fluorescent points were observed compared with the control (a), which indicates that the content of nitric oxide is increased. The fluorescent intensity of DAF-FM DA is proportional to the nitric oxide levels. As shown in Fig. 5F, exposure of SGC-7901 cell to 3.13 and 6.25 μM of complexes **1–4** led to an increase in DAF-FM DA fluorescence intensity of 1.80 and 5.27 times for **1**, 1.67 and 28.24 times for **2**, 7.82 and 20.08 times for **3**, 7.24 and 56.76 times for **4** than that of control, respectively. The increase in DAF-FM DA fluorescence intensity demonstrates that the complexes can increase the nitric oxide levels with a dose-dependent manner.

Detection of intracellular Ca^{2+} level

The mitochondria can store Ca^{2+}, but Ca^{2+} will overload under conditions of oxidative stress [46–48]. Increased intracellular Ca^{2+} concentration may be associated with apoptosis [49]. The intracellular Ca^{2+} concentration was measured by Molecular Devices using Fluo-3AM as fluorescent probe. Fluo-3AM combines with Ca^{2+} to be transferred into green fluorescent Fluo-3. The intracellular Ca^{2+} level in SGC-7901 cells induced by the complexes was determined under ImageXpress Micro XLS system and Multi Wavelength Cell Scoring module. As shown in Fig. 6A, in the control (a), weak green fluorescent points were found. After SGC-7901 cells were treated with 6.25 μM of complexes **1** (b), **2** (c), **3** (d) and **4** (e) for 24 h, bright green fluorescent points were observed, which indicated that the complexes can increase intracellular Ca^{2+} levels. The Flu-3 green fluorescence intensity is shown in Fig. 6B, SGC-7901 cells were exposed to different concentrations of complexes **1–4**, and the Flu-3 green fluorescent intensity increased compared with the control. This further confirms that the complexes can enhance the intracellular Ca^{2+} levels.

Detection of the release of cytochrome c from mitochondria

The release of cytochrome c (cyt-c) from the mitochondria into the cytosol of the cancer cells is the key event in the final steps leading to apoptosis [50, 51]. To investigate whether the complexes can release cytochrome c, the release of cytochrome c was examined by immunofluorescence
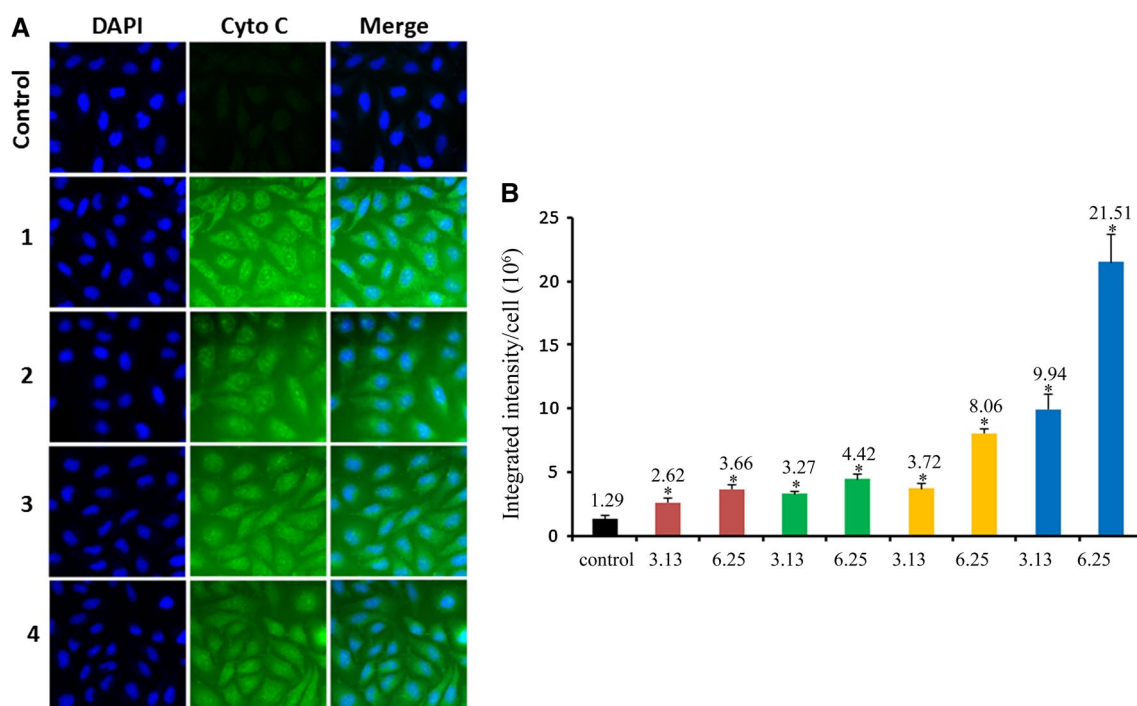
Fig. 7 **a** The release of cyt-c was examined after SGC-7901 cells were exposed to 12.5 μM of the complexes **1–4** for 24 h. **b** The integrated fluorescent intensity/cell was determined after differ-ent concentration of the complexes treated SGC-7901 cells for 24 h. $*P < 0.05$ represents significant differences compared with control
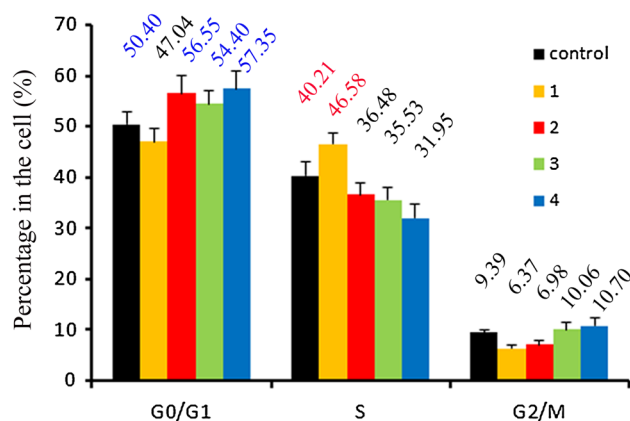

Fig. 8 The cell cycle distribution of SGC-7901 cells exposure to 12.5 μM of the complexes for 24 h

after treating the SGC-7901 cells with the complexes. As shown in Fig. 7A, after treatment of the SGC-7901 cells with 6.25 μM complexes **1–4** for 24 h, a number of green fluorescence was observed, which indicates that the complexes induce a release of cytochrome c from the mitochondria into the cytosol of the cytoplasm of SGC-7901 cells. However, no fluorescence of cytochrome c was found in the control cells. To quantitatively compare the efficiency of the

complexes **1–4** on the release of cytochrome c, the integrated green fluorescent intensity/cell was determined. As shown in Fig. 7B, exposure of SGC-7901 cells to 3.13 or 6.25 μM of complexes **1** (red), **2** (green), **3** (yellow) and **4** (blue) led to an increase in fluorescent intensity of cytochrome c compared with the control. Moreover, the green fluorescent intensity increases with the increase in concentration of the complexes. These data show that the complexes can release cytochrome c in a concentration-dependent manner.

Cell cycle arrest studies

The comet assay shows that the complexes can induce DNA damage, and the DNA damage causes the DNA damage pathway to be activated, leading to cell cycle arrest [52]. Inhibition of cancer cell proliferation by cytotoxic drugs could be the result of induction of apoptosis or cell cycle arrest, or a combination of these. The effect of the complexes on cell cycle progression of SGC-7901 cells was examined by flow cytometry. As shown in Fig. 8, in the control, the percentage of cells in the G0/G1 phase is 50.40%. After the treatment of SGC-7901 cells with 12.5 μM of complexes **2–4** for 24 h, cell cycle distribution analysis reveals that the percentage of cells in the G0/G1 phase is 56.55%, 54.40%, 57.35%, respectively. An increase in the percentage in the cell at G0/G1 phase of
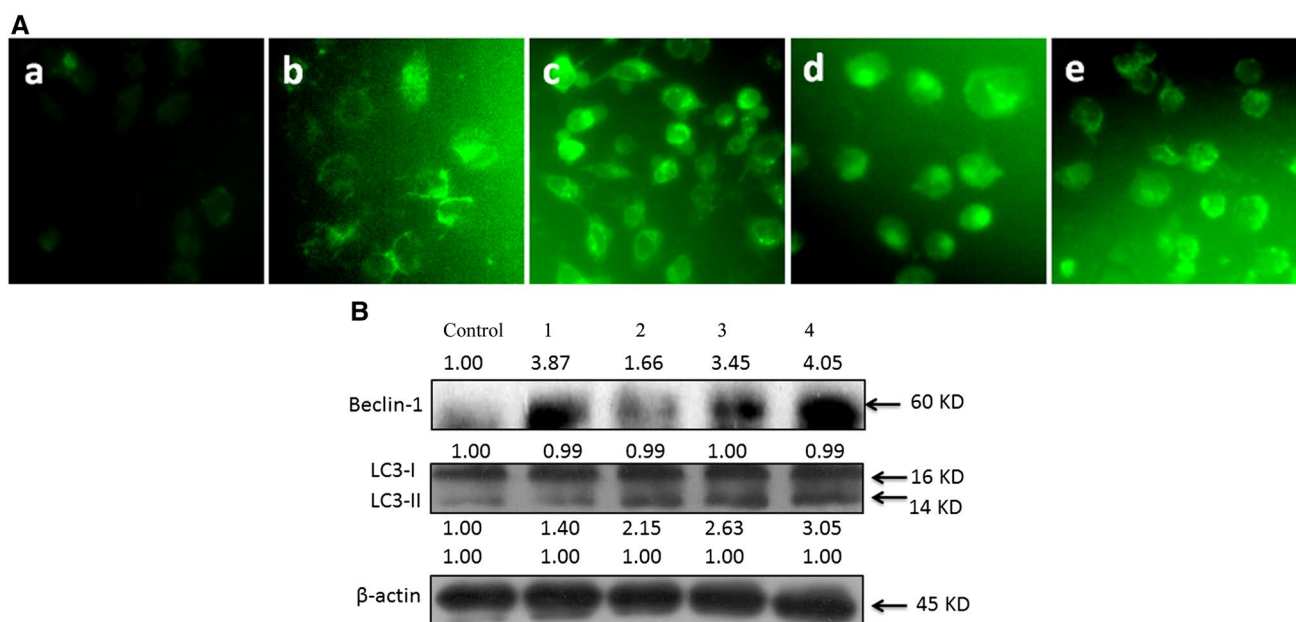
Fig. 9 A Autophagy was assayed after SGC-7901 cells (a) were treated with 6.25 μM of complexes **1** (b), **2** (c), **3** (d) and **4** (e) for 24 h. **B** The expression of Beclin-1 and LC3 was studied induced by 6.25 μM of complexes **1–4**
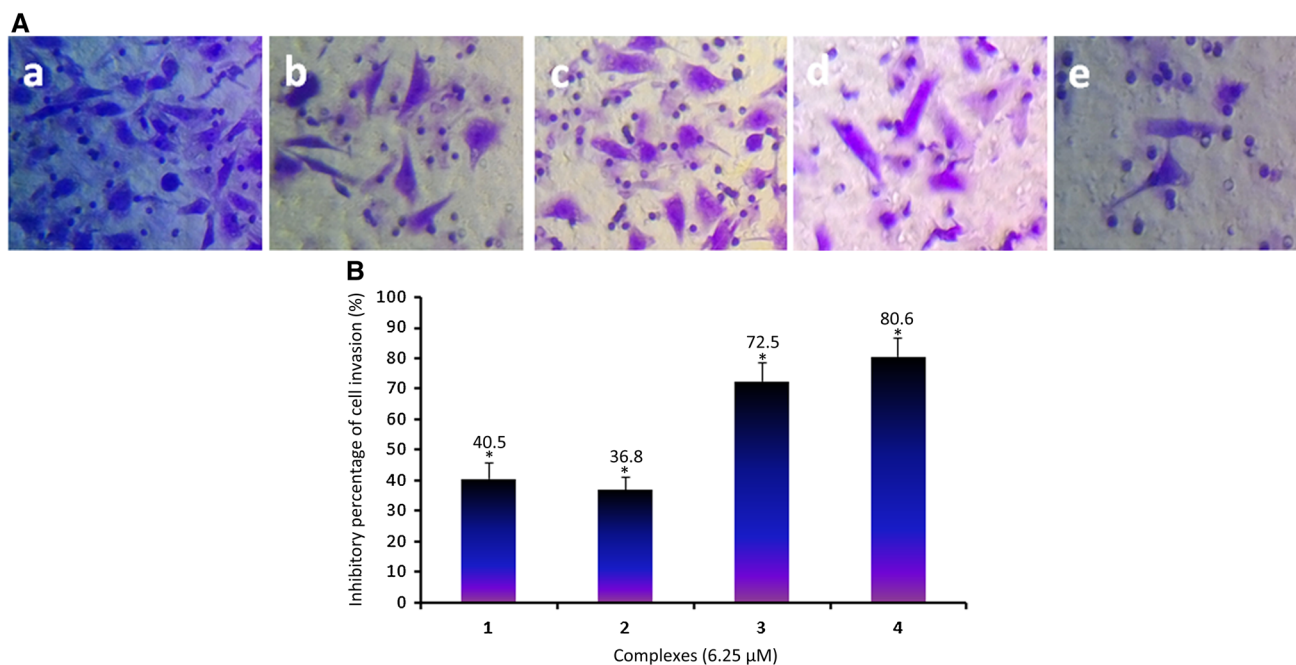

Fig. 10 A Microscope images of invading SGC-7901 cells (a) that have migrated through the Matrigel induced by 6.25 μM of complexes **1** (b), **2** (c), **3** (d) and **4** (e) for 24 h. **B** The inhibiting percentage of SGC-7901 cells invasion induced by 6.25 for 24 h. *$P < 0.05$ represents significant differences compared with control

6.15% for **2**, 4.00% for **3** and 6.95% for **4** was observed, which was accompanied by the corresponding reduction in the S phase. Thus, complexes **2**–**4** induce cell cycle arrest at G0/G1 phase. However, treatment with SGC-7901 cells with 12.5 μM of complex **1** resulted in an increase of 6.37% in the percentage of S phase, indicating that the complex **1** induced cell cycle arrest at S phase. The results reveal that complexes **1**–**4** inhibit the cell proliferation in SGC-7901 cells at G0/G1 or S phase.

Autophagy studies

Autophagy is a lysosomal degradation pathway, and it is essential for homeostasis under normal conditions [53]. Autophagy plays a key role in tissue homeostasis, development and cell death [54]. In order to investigate the autophagic effect of the complexes on SGC-7901 cells, the cells were treated with complexes **1**–**4** for 24 h, and then the cells were stained with monodansylcadaverine (MDC). It is well known that MDC is a marker for autophagic vacuoles [55]. As shown in Fig. 9A, in the control (a), no obvious green fluorescent points were observed. After SGC-7901 cells were incubated with 6.25 μM of complexes **1** (b), **2** (c), **3** (d) and **4** (e) for 24 h, a number of bright green fluorescent points were observed, which indicates that the complexes induce autophagy with the formation of autophagic vacuoles. In order to further confirm that the complexes can induce autophagy, some autophagy-related proteins were detected. One of the hallmarks of autophagy is the conversion of the soluble form of LC3 (LC3-I) to the lipidated and autophagosome-associated form (LC3-II) [56]. Beclin-1 is essential for the formation of autophagosomes. As shown in Fig. 9B, after SGC-7901 cells were treated with 6.25 μM of the complexes for 24 h, the protein expression of Beclin-1 and the LC3-II/LC3-I ratio was increased compared with the control. The results confirm that the complexes can induce autophagy in SGC-7901 cells.

Complexes inhibit invasion of SGC-7901 cells

To investigate the effect of the complexes on cell invasion, a transwell chamber assay was performed. As shown in Fig. 10A, in the control (a), SGC-7901 cells can freely move across the Matrigel toward the lower chamber of the transwell plate. On treatment of SGC-7901 cells with 6.25 μM of complexes **1** (b), **2** (c), **3** (d) and **4** (e) for 24 h, the extent of cell invasion decreases. The inhibiting percentage of cell invasion was also calculated. As shown in Fig. 10B, SGC-7901 cells were treated with 6.25 μM of complexes **1**–**4** for 24 h, and the percentage of inhibiting the cell invasion reaches 40.5%, 36.8%, 72.5% and
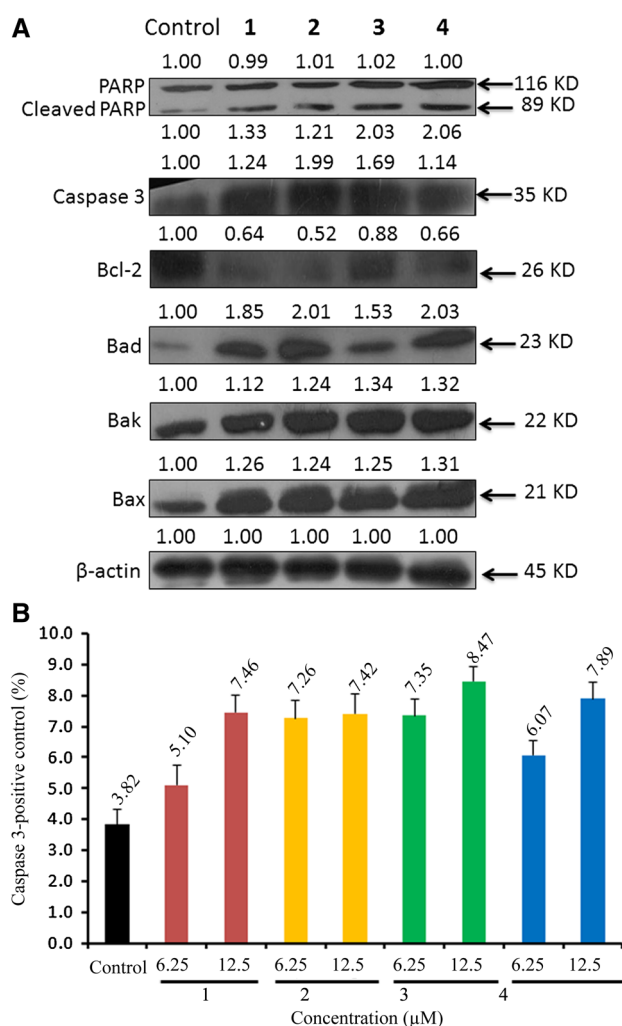

Fig. 11 **A** The expression of PARP, caspase-3 and Bcl-2 family proteins after SGC-7901 cells were exposed to 12.5 μM of the complexes **1**–**4** for 24 h. **B** Activation of caspase-3 was assayed after SGC-7901 cells were treated with 12.5 μM of complexes **1**–**4** for 24 h

80.6%, respectively. The inhibition of cell invasion follows the order of **4** > **3** > **1** > **2**. Complex **4** displays the highest inhibiting efficiency among the four complexes. Taken together, these results demonstrate that the complexes can effectively inhibit the cell invasion in SGC-7901 cells.

Activation of caspase-3 and expression of Bcl-2 family proteins

PARP cleavage is a hallmark of apoptosis. PARP plays an important role in biological processes, such as transcription and cell cycle regulation, response to DNA damage, apoptosis and maintenance of genome integrity [57]. The
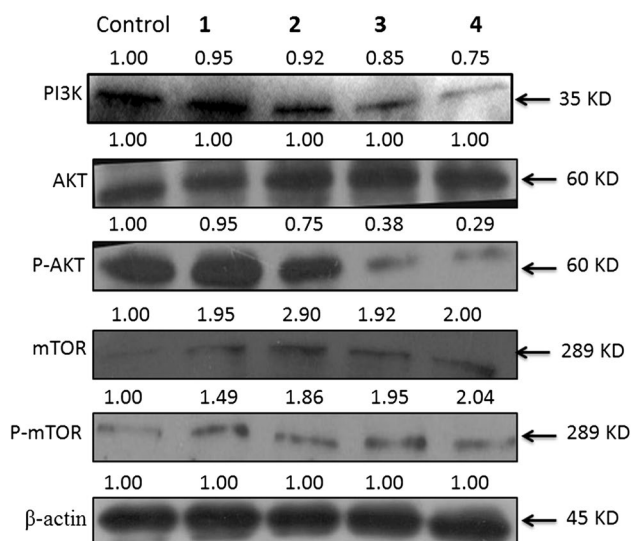
Fig. 12 Expression of PI3K, AKT, P-AKT and mTOR induced by 12.5 μM of the complexes for 24 h

caspase family is closely related to the cell apoptosis via the mitochondrial pathway [58]. And Caspase-3 activation is critical in the process of apoptosis [59]. As shown in Fig. 11A, the cleavage of PARP was observed after SGC-7901 cells were exposed to 12.5 μM of the complexes. In addition, the expression of caspase-3, proapoptotic proteins Bad, Bak and Bax was up-regulated, whereas the expression of antiapoptotic protein Bcl-2 was down-regulated. The stimulation of executioner caspases 3 was evaluated using fluorogenic inhibitor FLICA FAM-DEVD-FMK. FITC-DEVD-FMK is cell permeable, nontoxic

and irreversibly binds to activated caspase-3 in apoptotic cells. The FITC label allows for direction of activated caspases in apoptotic cells by flow cytometry. As shown in Fig. 11B, incubation of SGC-7901 cells with 12.5 μM of complexes **1**–**4** for 24 h led to an increase of 1.95 times for **1**, 1.92 times for **2**, 2.22 times for **3** and 2.07 times for **4** in the number of caspase-3-activated cells in comparison to the control, respectively. Furthermore, the complexes activate caspase-3 in a concentration-dependent manner.

Apoptotic mechanism studies

The PI3K/Akt signaling pathway is composed of a number of signal transduction molecules, including mechanistic targets of rapamycin (mTOR), phosphatase and tensin homolog (PTEN), AMP-activated protein kinase α (AMPKα), pyruvate dehydrogenase kinase-1 (PDK-1), 90 kDa ribosomal S6 kinase-1 (RSK1), eukaryotic translation initiation factor 4E-binding protein-1 (4E-BP1), glycogen synthase kinase-3α/β (GSK-3α/β), S6 ribosomal proteins, extracellular signal-regulated kinases (ERK-1/2), Bcl-2-associated death promoter (Bad) and protein 53 (p53) [60]. The evidence indicates that the PI3K/Akt pathway has a prominent role in multiple physiological and pathological processes, such as the cell cycle and apoptosis [61]. AKT is a downstream target of PI3K which regulates cellular survival, cell proliferation and protein synthesis in response to various extracellular stimuli [62]. The immunoblot was used to study the PI3K/Akt/mTOR signaling pathway. As shown in Fig. 12, with the exposure of SGC-7901 cells to 12.5 μM of complexes **1**–**4** for 24 h, the level of P-AKT was significantly decreased,

Fig. 13 The molecular mechanism of the complexes inducing apoptosis in SGC-7901 cells
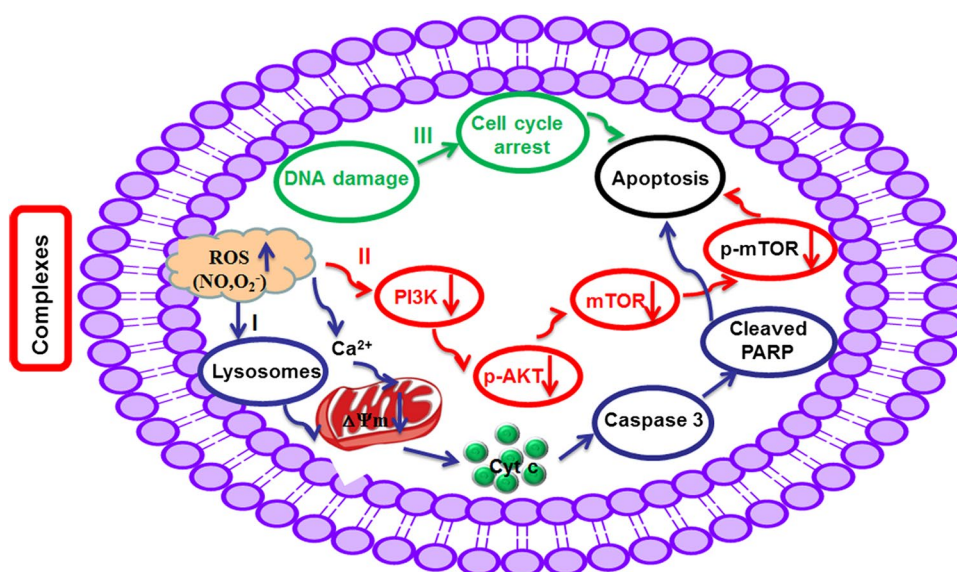
whereas the expression levels of mTOR and P-mTOR were up-regulated. These data indicate that the complexes **1**–**4** mediate the apoptosis and autophagy through inhibition of PI3K/AKT/mTOR signaling pathway.

Conclusions

Five new Ru(II) polypyridyl complexes **1**–**5** were synthesized and characterized. The complexes show high anti-cancer activity in vitro against SGC-7901 cells. Among the complexes, complexes **3** and **4** reveal higher cytotoxicity in vitro toward SGC-7901 cells than cisplatin under the same conditions. The apoptotic assays show that the complexes can induce apoptosis in SGC-7901 cells. The complexes **1**–**4** locate at the lysosome and cause lysosome membrane permeabilization after SGC-7901 cells were treated with the complexes for 6 h. However, after the incubation of SGC-7901 cells with the complexes for 8 h, the complexes enter into the mitochondria and can induce a decrease in mitochondrial membrane potential. Additionally, the complexes can increase intracellular ROS and Ca^{2+} levels and induce a release of cytochrome c. The Western blot suggests that the complexes activate caspase 3, cleave PARP, down-regulate the expression of Bcl-2 protein and up-regulate the expression of Bad, Bak and Bax proteins. In summary, the complexes induce apoptosis through the following three pathways (Fig. 13): (1) ROS-mediated lysosome–mitochondria dysfunction pathway; (2) inhibition of PI3K/AKT/mTOR pathway; and (3) Damage of DNA and inhibition of the cell growth at G0/G1 or S phase pathway.

References

1. Boerner LJ, Zaleski JM (2005) Curr Opin Chem Biol 9:135–144
2. Palermo G, Magistrato A, Riedel T, Von Erlach T, Davey CA, Dyson PJ, Rothlisberger U (2015) ChemMedChem 11:1199–1210
3. Markman M (2003) Expert Opin Drug Saf 2:597–607
4. Bruijnincx PC, Sadler PJ (2008) Curr Opin Chem Biol 12:197–206
5. Chen JC, Peng F, Zhang Y, Li BJ, She J, Jia XM, Zou ZL, Chen M, Chen LM (2017) Eur J Med Chem 140:104–117
6. Kaulage MH, Maji B, Pasadi S, Buattacharya S, Muniyappa K (2017) Eur J Med Chem 139:1016–1029
7. Wan D, Tang B, Wang YJ, Guo BH, Yin H, Yi QY, Liu YJ (2017) Eur J Med Chem 139:180–190
8. Zeng CC, Lai SH, Yao JH, Zhang C, Yin H, Li W, Han BJ, Liu YJ (2016) Eur J Med Chem 122:118–126
9. Wang JQ, Kou JF, Zhao ZZ, Qiu KQ, Chao H (2017) Inorg Chem Front 4:1003–1012
10. Cao Q, Li Y, Freisinger E, Qin PZ, Sigel RO, Mao ZW (2017) Inorg Chem Front 4:10–32
11. Deepika N, Kumar YP, Devi CS, Reddy PV, Srishailam A, Satyanarayana S (2013) J Biol Inorg Chem 18:751–766
12. Zhang C, Han BJ, Zeng CC, Tang B, Wan D, Jiang GB, Liu YJ (2016) J Inorg Biochem 157:62–72
13. Sainuddin T, McCain J, Pinto M, Yin H, Gibson J, Hetu M, McFarland SA (2016) Inorg Chem 55:83–95
14. Oliveira KM, Liany LD, Corrêa RS, Deflon VM, Comineth MR, Bitastia AA (2017) J Inorg Biochem 176:66–76
15. Chen WX, Song XD, Hu SF, Sun J, Chen JX, Wu T, Mao ZW (2016) J Inorg Biochem 64:91–98
16. Milutinović MM, Rilak A, Bratsos L, Klisurić O, Vraneŝ M, Gligorijević N, Radelović S, Bugarčić ŻD (2017) J Inorg Biochem 169:1–12
17. Li GY, Sun LL, Ji LN, Chao H (2016) Dalton Trans 45:13261–13276
18. Du KJ, Liang JW, Kou JF, Qian C, Ji LN, Chao H (2014) Dalton Trans 43:17303–17316
19. Tang B, Han BJ, Wan D, Lai SH, Wang XZ, Zhang C, Zeng CC, Liu YJ (2017) Transit Met Chem 42:373–396
20. Li W, Jiang GB, Yao JH, Wang XZ, Wang J, Han BJ, Xie YY, Lin GJ, Huang HL, Liu YJ (2014) J Photochem Photobiol B Biol 140:94–104
21. Wan D, Lai SH, Zeng CC, Zhang C, Tang B, Liu YJ (2017) J Inorg Biochem 173:1–11
22. Lai SH, Jiang GB, Yao JH, Li W, Han BJ, Zhang C, Zeng CC, Liu YJ (2015) J Inorg Biochem 152:1–9
23. Cao WQ, Zheng WJ, Chen TF (2015) Sci Rep 5:9157
24. Deepika N, Devi CS, Kumar YP, Reddy KL, Reddy PV, Kumar DA, Singh SS, Satyanarayana S (2016) J Photochem Photobiol B Biol 160:142–153
25. Juris A, Balzani V, Barigelletti F, Campagna S, Belser P, Von Zelewsky A (1988) Coord Chem Rev 84:85–277
26. Habtemariam A, Melchart M, Fernandez R, Parsons S, Oswald IDH, Parkin A, Fabbiani FPA, Davidson JE, Dawson AE, Aird RE, Jodrell DI, Sadler PJ (2006) J Med Chem 49:6858–6868
27. Sun B, Wang YC, Qian C, Chu J, Liang SM, Chao H, Ji LN (2010) J Mol Struct 963:153–159
28. Sullivan BP, Salmon DJ, Meyer TJ (1978) Inorg Chem 17:3334–3341
29. Collin JP, Sauvage JP (1986) Inorg Chem 25:135–141
30. Mosmann T (1983) J Immunol Methods 65:55–63
31. Lo KK, Lee TK, Lau JS, Poon WL, Cheng SH (2008) Inorg Chem 47:200–208
32. Alapetite C, Wachter T, Sage E, Moustacchi E (1986) Int J Radiat Biol 69:359–369
33. Franco JL, Posser T, Dunkley PR (2009) Free Radic Biol Med 7:449–457
34. Wang X, Nguyen DM, Yanez CO, Rodriguez L, Ahn HY, Bondar MV, Belfield KD (2010) J Am Soc Chem 132:12237–12239
35. Chang Y, Li Y, Ye N, Guo X, Li Z, Sun G, Sun Y (2016) Apoptosis 21:977–996
36. Zhong Y, Jin C, Gan J, Wang X, Shi Z, Xia X, Peng X (2017) Toxicon 130:106–113
37. Yugandhar D, Nayak VL, Archana S, Shekar KC, Srivastava AK (2015) Eur J Med Chem 101:348–357
38. Prasad S, Gupta SC, Tyagi AK (2017) Cancer Lett 387:95–105
39. Ozben T (2007) J Pharm Sci 96:2181–2196
40. Shadel GS, Horvath TL (2015) Cell 163:560–569
41. Gammella E, Recalcati S, Cairo G (2016) Oxid Med Cell Longev 2016:8629024
42. Diebold L, Chandel NS (2016) Free Radic Biol Med 100:86–93
43. Zorov DB, Juhaszova M, Sollott SJ (2014) Physiol Rev 94:909–950
44. Shen HM, Liu ZG (2006) Free Radic Biol Med 40:928–939
45. Dröge W (2002) Physiol Rev 82:47–95

46. Romagnoli A, Aguiari P, De SD, Leo S, Marchi S, Rimessi A, Zecchini E, Pinton P, Rizzuto R (2007) Endoplasmic reticulum/mitochondria calcium cross-talk. Novartis Found Symp 287:122–131

47. Duszyński J, Kozieł R, Brutkowski W, Szczepanowska J, Zabłocki K (2006) BBA Bioenerg 1757:380–387

48. Trump BF, Berezesky IK (1995) FASEB J 9:219–228

49. Orrenius S, Zhivotovsky B, Nicotera P, Orrenius S, Zhivotovsky B, Nicotera P (2003) Nat Rev Mol Cell Biol 4:552–565

50. Renz A, Berdel WE, Kreuter M, Belka C, Schulze-Osthoff K, Los M (2001) Blood 98:1542–1548

51. Osaka A, Hasegawa H, Yamada Y, Yanagihara K, Hayashi T, Mine M, Aoyama M, Sawada T, Kamihira SA (2009) J Cancer Res Clin Oncol 135:371–377

52. Alghamian Y, Abou AG, Murad H, Madania A (2017) Adv Med Sci 62:330–337

53. Okada H, Mak TW (2004) Nat Rev Cancer 4:592–603

54. Tiwari RV, Parajuli P, Sylvester PW (2015) Mol Cell Biochem 408:1–15

55. Biederbick A, Kern HF, Elsässer HP (1995) Eur J Cell Biol 66:3–14

56. Rubinsztein DC, Gestwicki JE, Murphy LO, Klionsky DJ (2007) Nat Rev Drug Discov 6:304–312

57. Duriez PJ, Shah GM (1997) Biochem Cell Biol 75:337–349

58. Hara K, Kasahara E, Takahashi N, Konishi M, Inoue J, Jikumaru M, Kubo S, Okamura H, Sato E, Inoue M (2011) J Pharmacol Exp Ther 337:838–845

59. Danial NN, Korsmeyer SJ (2004) Cell 116:205–219

60. Kilic U, Caglayan AB, Beker MC, Gunal MY, Caglayan B, Yalcin E, Kelestemur T, Gundogdu RZ, Yulug B, Yılmaz B, Kerman BE, Kilic E (2017) Redox Biol 12:657–665

61. Tapia-Limonchi R, Cahuana GM, Caballano-Infantes E, Salguero-Aranda C, Beltran-Povea A, Hitos AB, Hmadcha A, Martin F, Soria B, Bedoya FJ, Tejedo JR (2016) J Cell Biochem 117:2078–2088

62. Song G, Ouyang G, Bao S (2005) J Cell Mol Med 9:59–71